Improving Operational Radar Rainfall Estimates Using Profiler Observations Over Complex Terrain in Northern California

Haonan Chen, *Member, IEEE*, Robert Cifelli, and Allen White

***Abstract*— Quantitative precipitation estimation (QPE) using operational weather radars in the western United States is still a challenging issue due to the beam blockage in the mountainous areas and complex rainfall microphysics induced by the orographic enhancement. This article aims to improve operational radar rainfall estimates in complex terrain by incorporating auxiliary remote sensing observations. An innovative vertical profile of reflectivity (VPR) correction scheme is developed for operational radar using observations from multiple vertically pointing profilers to represent the vertical structure of precipitation at various locations. A demonstration study in the Russian River basin in Northern California is detailed. Results show that the QPE performance is significantly improved after VPR correction, and this new VPR correction approach is superior to the conventional approach currently applied in the operational radar rainfall system. The normalized standard error of hourly rainfall estimates for the two precipitation events presented in this article is improved by ∼20% after applying the proposed VPR correction scheme.**

***Index Terms*— Complex terrain, quantitative precipitation estimation (QPE), S-band vertically pointing profiler (S-PROF), vertical profile of reflectivity (VPR) correction, weather radar.**

I. Introduction

THE National Weather Service (NWS) Weather Surveillance Radar—1988 Doppler (WSR-88D) systems form the cornerstones of national severe weather warning and forecast infrastructure. However, quantitative precipitation estimation (QPE) using operational WSR-88D over the western United States remains a formidable challenge because of the mountainous topography [1]–[4]. The limitations of radar sampling geometry are further compounded by the complex precipitation microphysics as a result of land–ocean interaction in the coastal zones and orographic enhancement in the mountainous regions [5], [6]. This article aims to improve the WSR-88D-based rainfall estimates by incorporating auxiliary observations from vertically pointing profiler radars. The Russian River basin near the San Francisco Bay Area (hereafter referred to as Bay Area) in Northern California is used as the demonstration domain.

The Bay Area is mainly covered by two WSR-88D radars: KMUX and KDAX. The KDAX radar is located near Davis, CA, USA, over 80 km from the closest portion of the Russian River basin. The KDAX radar beams are also partially blocked at the lowest two elevation angles (i.e., 0.5° and 0.9°). The KMUX radar is located in the Santa Cruz Mountains, over 150 km to the basin. In addition, KMUX is deployed at an elevation of over 1000 m compared with the Russian River valley which is near sea level [7]. There is another WSR-88D (i.e., KBBX) providing partial coverage to the Russian River watershed, which is located further north in the Beale Air Force Base, east of Marysville, CA, USA. But the KBBX radar is over 120 km from the closest boundary of the watershed, and it is much further from the Bay Area. Typically, the storms in Northern California have freezing levels approximately 1–2-km above ground level (AGL). Due to the beam broadening and height increase with a range, the WSR-88D radar sampling volumes may be partially or completely filled with either the mixed-phase hydrometeors in the bright band (BB) or snowflakes above the BB [see Fig. 1(a)] even if it is raining at the ground. If the radar sampling volume is above the BB, the corresponding observations will induce significant underestimation in precipitation estimates on the ground. If the radar is sampling within the BB, the enhanced reflectivity due to the melting of aggregated snow will cause overestimation in radar QPE.

A number of studies have focused on the mitigation of radar QPE errors associated with the nonuniform vertical profile of reflectivity (VPR) in the BB and the solid precipitation region above the BB. A common approach suggested to account for this effect is to correct the measured reflectivity profiles using *a priori* information on the VPR and then apply the radar rainfall estimators based on the corrected reflectivity. In particular, the reflectivity measured aloft is revised in a mean sense to an expected reflectivity near the ground level [8], which is ultimately used to calculate QPE using a Z–R relationship. Several VPR correction schemes have been proposed in the literature. For example, Kitchen *et al.* proposed a physically based strategy to construct an idealized reflectivity profile from radar range height indicator (RHI)

Manuscript received March 25, 2019; revised September 2, 2019; accepted October 20, 2019. Date of publication November 12, 2019; date of current version February 26, 2020. This work was supported in part by the California Department of Water Resources, in part by the Sonoma County Water Agency, and in part by the Physical Sciences Division of the National Oceanic and Atmospheric Administration (NOAA) Earth System Research Laboratory. *(Corresponding author: Haonan Chen.)*

H. Chen is with the Cooperative Institute for Research in the Atmosphere (CIRA), Colorado State University, Fort Collins, CO 80523 USA, and also with the Physical Sciences Division (PSD), NOAA Earth System Research Laboratory, Boulder, CO 80305 USA (e-mail: haonan.chen@noaa.gov).

R. Cifelli and A. White are with the Physical Sciences Division (PSD), NOAA Earth System Research Laboratory, Boulder, CO 80305 USA.

Color versions of one or more of the figures in this article are available online at http://ieeexplore.ieee.org.

Digital Object Identifier 10.1109/TGRS.2019.2949214

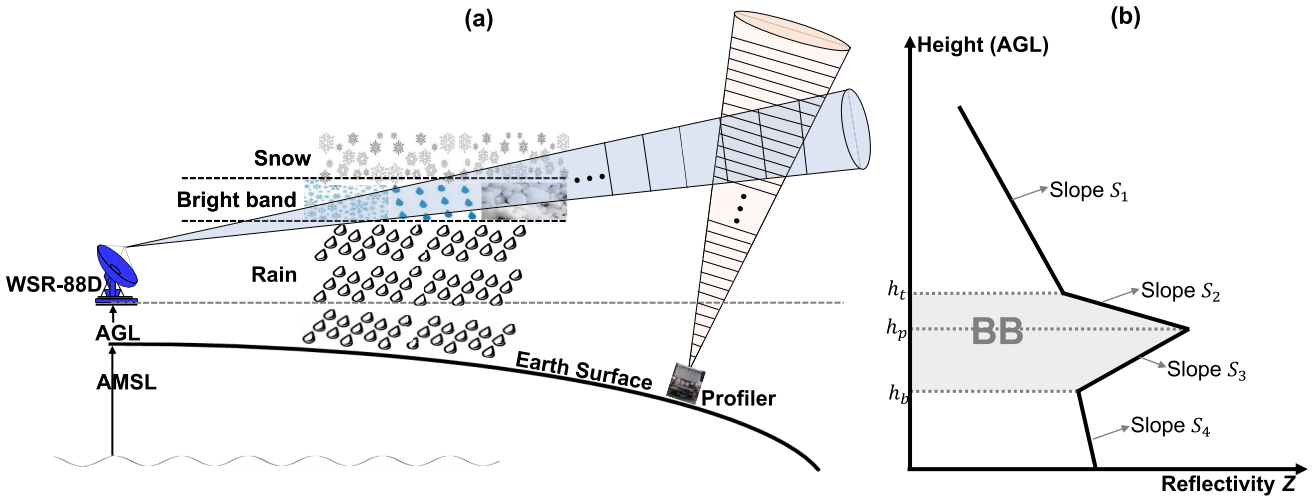

Fig. 1. (a) Diagram illustrating the sampling limitations of WSR-88D in Northern California. (b) Idealized model of VPR: h_p stands for the BB peak, and the region between BB bottom h_b and BB top h_t indicates the reflectivity enhancement due to the melting of aggregated snow above the BB or mixed-phase hydrometeors in the BB.

scans during a total of 112 days over a three-year period [9]. The idealized VPR was weighted by the radar beam power profile to calculate the reflectivity factor which should be observed. The calculated reflectivity factor was then compared with the actual radar measurement, and the profile was adjusted to compensate for the BB effect in an iterative way until the calculated reflectivity and the measured reflectivity agree within an acceptable tolerance [9]. Andrieu and Creutin [10] formulated a statistical model of VPR using radar data at two elevation angles. This model also relies on the existence of a mean VPR representative of the vertical structure of reflectivity in the domain of interest. Germann and Joss [11] developed an adaptive mesobeta-scale solution to VPR correction for each scan elevation angle through the representative VPR estimated by averaging radar measurements from a 70-km radius cylinder centered over the radar site. Bellon *et al*. [12] evaluated two VPR correction schemes, namely near-range VPR and intensity-dependent "climatological" VPR, using simulations in order to isolate the VPR effects as a function of BB height, uncertainties in the BB height, as well as the averaging area. Matrosov *et al*. [8] used the polarimetric radar measurements of ρ_{hv} to identify the BB location on a beam-to-beam basis and then corrected the reflectivity profiles based on the mean VPR at a certain range derived from the RHI scans. Zhang and Qi [13] attempted to identify the BB according to radar reflectivity distribution and temperature data from a nearby sounding station. Then, the mean VPR in the BB area is computed from the volume scan radar reflectivity measurements and fitted using a linear model. The idealized linear VPR model is used to correct for BB effect in the measured reflectivity. This approach is applied in the operational multiradar–multisensor (MRMS) system [14]. Koistinen and Pohjola [15] tried to estimate the ground-level reflectivity using two VPR-based correction ensembles, respectively, derived from the measured and parameterized reflectivity profiles. In particular, the first ensemble contained 24 members based on the measured average VPRs derived from the volume scans at 15-min intervals during the most recent 6 h, whereas the second ensemble contained 24 members similarly but from the parameterized climatological VPRs.

These correction methodologies can be roughly classified into two categories according to the VPRs used in the correction: 1) long-term climatological VPR and 2) short-term observed VPR. In summary, the climatological VPRs are obtained from radar observations averaged over a certain area and over a long time period, whereas the short-term observed VPRs are typically obtained from multiple elevations of one or several volume scan data for a wide area. Both the long-term and short-term data can be used to model the idealized VPR representative, as shown in Fig. 1(b). Therein, a number of VPR model parameters are estimated, including BB top h_t, BB peak height h_p, BB bottom h_b, and slopes of S_1, S_2, S_3, and S_4. However, the climatological VPR cannot represent the temporal and spatial variations in the vertical structure of precipitation. The short-term VPR can better capture the temporal variations but not the spatial variabilities. In addition, most of the previous studies concentrated on rather flat domains with a little variation in the vertical structure of precipitation. In complex terrain such as the Northern California, in addition to the moisture and/or cloud condensate, wind direction and terrain forcing are the key factors affecting the precipitation intensity and distribution [5]. Conventional VPR correction schemes may not be sufficient to capture the environmental variations as such. Furthermore, due to the terrain blockage and low freezing levels, it is challenging to collect sufficient low-level observations to construct a complete representative VPR model for the correction of upper-level measurements from the operational WSR-88D radar.

Qi *et al*. [16] attempted to use observations from two vertically pointing profilers to correct WSR-88D measurements for QPE in complex terrain. In particular, two sets of reference VPRs are derived using the two profilers; one for the coastal mountains and the other for the Sierra Nevada. Each represented a large area (i.e., a single VPR was constructed

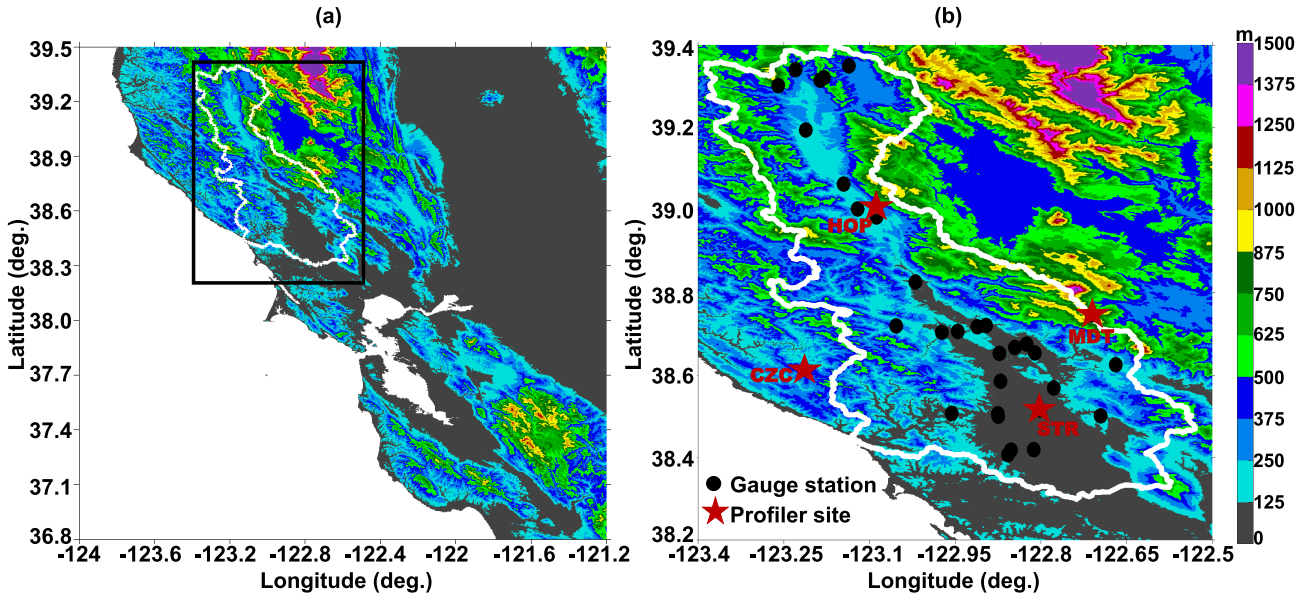

Fig. 2. (a) DEM information of the San Francisco Bay Area (Northern California). The Russian River basin boundaries are highlighted in white. (b) DEM information of the rectangular area (Russian River watershed) indicated in (a). The black dots denote rain gauge locations, where the four sites marked with pentagrams are equipped with vertically pointing profilers, which will be used to represent the VPR features in this area.

for an area about 200 km × 200 km in the coastal mountain region). Although a consistent improvement on WSR-88D QPE was observed during the three heavy rainfall events detailed in their study, the VPR correction approach in [16] has severe limitations when there are large horizontal variabilities in the precipitation distribution. In addition, [16] assumed a fixed "ideal" VPR model to represent the vertical precipitation structure over a large spatial–temporal domain, similar to most of the previous studies. The profiler data were not dynamically utilized to resolve the changing precipitation structures. This article develops an innovative VPR correction scheme for WSR-88D radars based on the auxiliary remote sensing observations from multiple vertically pointing profiler radars deployed over complex terrain. In particular, four S-band vertically pointing profilers (S-PROFs) are used to investigate and represent the vertical structure of precipitation at various locations in or near the Russian River watershed. The multiprofiler observations, which can better characterize small-scale rainfall microphysical processes, are directly and dynamically incorporated in the WSR-88D data processing and subsequent derivation of rainfall products.

The remainder of this article is organized as follows. Section II details the study domain, instrumentation, and VPR correction methodology. Section III presents two case studies, as well as the performance evaluation of the proposed VPR correction scheme in terms of QPE. The main findings of this article and operational implementation challenges are summarized in Section IV.

II. Study Domain, Instrumentation, and Methodology

A. Study Domain

In this article, the Russian River basin is used as a demonstration study domain. The Russian River watershed is located within Sonoma and Mendocino Counties in Northern California. Fig. 2 shows the detailed terrain information within this watershed. It is roughly 130 km long, drains 3846 km^2, and has an average annual discharge of 2 km^3. This watershed includes several world-renowned vineyards and the winemaking industry that dominates the local economy. It is one of the most flood-prone areas in the state of California because of the watershed's unique geography and its exposure to atmospheric rivers (ARs) [17]. ARs are long and narrow regions of intense water vapor transport that can produce heavy wintertime rainfall, resulting in floods, mudslides, and debris flows [17]–[19].

On the other hand, Northern California, including the Russian River watershed, relies on a few AR events every year to replenish water supply reservoirs. Water supply in the Russian River is further impacted by diversions for vineyard irrigation and frost protection, which continue to expand in response to high-value wine industry demands. In addition, endangered salmon fisheries require tributary and mainstream flows during the late summer and early fall spawning season when precipitation is scarce and agriculture, recreation, and other water supply demands are high. Therefore, accurate QPE is critical to inform the decision process for water managers that are balancing the competing needs for water supply and flood mitigation. However, it is very difficult to obtain reliable QPE for this region due to the challenges posed by the sampling limitations of WSR-88D and complex precipitation microphysics resulting from orographic enhancement [3]. Currently, the NWS California Nevada River Forecast Center (CNRFC) does not use radar information to derive the mean areal precipitation that is used to drive the NWS River Forecast System (NWSRFS) for the Russian River watershed. It only relies on the rain gauge data and rainfall climatology in this mountainous region. To this end, this article aims to improve

TABLE I
SPECIFICATIONS OF THE NOAA S-BAND PROFILER RADAR (FROM [21])

Frequency	2.875 GHz
Antenna diameter	2.4 m
Average transmit power	20 W
Peak power	360 W
Beamwidth	2.5°
Range resolution	45, 60, 105, 420 m
Height of the lowest gate	142 or 159 m
Time resolution, nominal	30 s
Doppler technique	FFT
Sensitivity	-14 dBZ at 10 km

the operational radar-based QPE, which can result in better flood forecasting and protection of aquatic ecosystems in the vicinity of this particular domain.

B. Instrumentation

The data sets used in this article include a combination of operational WSR-88D, vertically pointing profiler radars, and surface rain gauge measurements. In particular, we take advantage of the unique observations from the legacy of the National Oceanic and Atmospheric Administration (NOAA) Hydrometeorology Testbed (HMT) [20].

1) Selection of WSR-88D Radar: As mentioned, there are three WSR-88D radars providing partial or full coverage to the Russian River watershed, namely, KDAX, KBBX, and KMUX, which are, respectively, about 80, 120, and 150 km from the closest boundary of the basin. The KMUX and KBBX radars cannot provide adequate coverage to the area of interest because of the longer distances and considerable blockage. Though the lowest two beams are partially blocked by the coastal mountains, the higher beam tilts and hybrid scans from the KDAX radar can still provide lower level observations than the radar KMUX or the KBBX radar. Therefore, the KDAX radar is often used to obtain QPE over this terrain. For example, the operational MRMS radar-only product over the watershed is predominantly derived from the KDAX radar observations [2], [3]. Therefore, we selected the KDAX radar for the demonstration of the proposed VPR correction scheme. Particularly, the third tilt (1.3° elevation angle) scans are used to derive QPE since it is the lowest beam that is not affected by the partial blockage. The choice of the KDAX radar also facilitates cross comparison with the operational rainfall products from the MRMS system.

2) NOAA Profiler Data: In order to capture the vertical structure of precipitation, this article utilizes the unique observations from several NOAA S-PROFs [21]. The S-PROF are designed to continuously monitor precipitation evolution overhead at relatively high temporal and vertical resolutions and have been used in a number of previous studies (see [5], [16], [22]–[24]). The key specifications of the S-PROF are listed in Table I. The interested readers may refer to White *et al*. [21] for more details about the profiler system.

In particular, four S-PROFs were deployed in the vicinity of the Russian River watershed (see Fig. 2) as part of the NOAA HMT program and used in this article to study rainfall variability across the watershed. Table II details the locations of the S-PROF and their relative position to the KDAX radar. The high-resolution S-PROF data are used to construct the local VPR structures at different types of terrain.

3) Rain Gauge Data: Rainfall measurements from automatic weather stations are used to demonstrate the proposed VPR correction technique in terms of QPE. As shown in Fig. 2, there are 35 NOAA gauge sites deployed within the Russian River basin. The locations of these gauges and their distances to the KDAX radar are shown in Table III. Table III also illustrates the sampling geometry of the KDAX radar's 1.3° elevation scan at each gauge station, including the beam direction and the height of the beam center. Among the 35 gauges, four are collocated with the above-described S-PROF. At each station, the rainfall data are archived when a tip (i.e., 0.254 mm) occurs and the data are stored at 2-min intervals. For the sake of cross comparison with the operational MRMS product, the gauge data are aggregated to accumulations at an hourly scale at the top of each hour.

C. VPR Correction Methodology

It should be noted that the WSR-88D radar scans over a wide area, whereas the S-PROF provides vertical profiles at a single location. As noted in Section I, traditional studies used a single-representative VPR to correct scanning radar measurements at large spatial scales, which completely neglected the spatial variations of precipitation. In complex terrain such as the Russian River watershed, such assumption may not be sufficient. The novelty of the VPR correction scheme presented in this article lies in the utilization of multiple S-PROFs to observe the vertical structure of precipitation in different subbasins of the Russian River watershed. Instead of using a single VPR model to represent the whole watershed, the auxiliary vertical measurements can better resolve the spatial variability of precipitation in complex terrain resulting from changes in the precipitation patterns on windward and leeward slopes and in the valley regions.

1) Delineating the Watershed: In order to represent the spatial distribution of precipitation at subbasin scales, we built upon an existing geographic information system (GIS) database of the Russian River basin. For the sake of implementation, the watershed is divided into four subdomains based on the hydrologic characteristics and the locations of the S-PROF. The vertical precipitation features in each individual subdomain are represented by the measurements from an individual S-PROF.

In order to distinguish the boundaries of the four subdomains, we first use the digital elevation model (DEM) information to locate the rivers, lakes, and streams over the Russian River watershed. Then, the flow directions are derived using the methodology proposed by Jenson and Domingue [25]. Therein, the direction of flow is determined as the direction of steepest descent. Then, the ArcGIS Watershed tool is adopted to process the flow directions and delineate subwatersheds. The identification of subwatersheds relies considerably on the techniques commonly used in data mining. In particular, an adaptation of the K-means clustering algorithm is applied

TABLE II

LOCATION OF THE KDAX SCANNING RADAR AND VERTICALLY POINTING PROFILERS. (FROM LEFT TO RIGHT) COLUMNS REFER TO THE STATION ID, LATITUDE (°N), LONGITUDE (°W), ELEVATION ABOVE MEAN SEA LEVEL (AMSL: m), AND CORRESPONDING AZIMUTHAL ANGLE (°) AND RANGE (km) FROM THE KDAX RADAR, AS WELL AS THE COUNTIES WHERE THE RADARS ARE DEPLOYED

Station ID	Latitude	Longitude	Elv.	Azimuth, Range	City, County
Scanning WSR-88D Radar					
KDAX	38.5011	-121.6778	41.6	0, 0	Davis, Yolo County
Vertically-pointing Profiler Radars					
HOP	39.0000	-123.0900	253	294.8, 134.4	Hopland, Mendocino County
MDT	38.7456	-122.7112	972	287.2, 93.8	Middletown, Lake County
STR	38.5154	-122.8022	32	271.3, 97.9	Santa Rosa, Sonoma County
CZC	38.6107	-123.2152	478	275.7, 134.2	Cazadero, Sonoma County

TABLE III

NOAA HMT GAUGE STATIONS USED FOR RADAR QPE VERIFICATION IN THIS ARTICLE. (FROM LEFT TO RIGHT) COLUMNS REFER TO THE STATION ID, LATITUDE (°N), LONGITUDE (°W), ELEVATION AMSL (m), CORRESPONDING AZIMUTHAL ANGLE OF THE KDAX RADAR SCAN (°), DISTANCE TO THE KDAX RADAR (km), AND CENTER HEIGHT OF THE KDAX RADAR'S 1.3° BEAM AT EACH GAUGE STATION (m)

ID	Lat	Long	Elv	Azi	Ran	Ht
HDS	38.5856	-122.8706	27	275.5	104.4	3090.1
BTO	38.4199	-122.8130	29	265.2	99.5	2912.2
STR	**38.5154**	**-122.8022**	**32**	**271.3**	**98.1**	**2859.5**
ROD	38.5073	-122.9565	39	270.8	111.5	3338.6
DUT	38.4074	-122.8580	41	264.6	103.5	3043.6
GTT	38.4181	-122.8522	50	265.2	102.9	3012.9
HDN	38.6538	-122.8104	51	280.1	100.1	2911.5
RVO	38.6668	-122.8460	55	280.6	103.4	3026.0
PIC	38.6754	-122.8250	58	281.3	101.8	2965.4
GSW	38.7042	-122.9732	58	281.7	115.1	3454.2
HOF	38.7173	-122.9110	66	283.0	110.1	3259.8
SRN	38.5060	-122.8755	68	270.7	104.5	3052.8
GSN	38.7205	-122.8959	68	283.3	108.9	3213.5
HBG	38.6530	-122.8732	70	279.6	105.5	3087.1
SHO	38.5007	-122.8750	73	270.3	104.4	3044.1
GYM	38.7060	-122.9460	79	282.0	112.8	3347.0
OCL	38.3849	-122.9357	85	263.7	110.6	3259.3
WNE	38.5688	-122.7773	91	274.8	96.2	2733.4
CLN	38.8252	-123.0200	99	287.5	122.2	3683.6
KLG	38.6249	-122.6692	151	279.3	87.5	2372.4
STN	38.5009	-122.6958	157	270.3	88.8	2410.7
HLD	39.0030	-123.1209	164	294.4	137.3	4215.3
HLN	39.0627	-123.1453	167	296.5	141.9	4400.0
HLE	38.9828	-123.0878	168	294.0	133.7	4066.4
UKN	39.1941	-123.2116	201	300.5	153.8	4864.2
HOP	**39.0000**	**-123.0900**	**253**	**294.7**	**134.7**	**4021.5**
RVN	39.3406	-123.2297	294	305.2	124.2	3565.9
POV	39.3492	-123.1366	305	307.1	157.7	4927.5
LSN	38.7187	-123.0537	396	281.8	122.2	3386.6
CZC	**38.6107**	**-123.2152**	**478**	**275.7**	**134.6**	**3792.4**
PVW	39.3204	-123.1802	518	305.4	158.9	4766.3
RVE	39.3143	-123.1869	520	305.1	159.0	4768.7
WLS	39.3463	-123.3166	594	304.0	170.3	5192.4
RVW	39.3014	-123.2601	631	303.4	163.5	4853.9
MDT	**38.7456**	**-122.7112**	**972**	**287.1**	**94.0**	**1775.4**

to incorporate the spatial contiguity of the terrain information. Ten subwatersheds are identified first (this number is inferred from the ArcGIS Watershed tool). Then, four connected regions within the watershed are derived [see Fig. 3(b)] based on the locations of the S-PROF using a connected component labeling (CCL) algorithm [26].

One of the distinguishing points of the proposed VPR correction scheme is that the correction is performed individually over the four connected regions. However, it should be noted that the split of the watershed in this article is essentially based on the hydrologic features and terrain elevations (above sea level). It may not be sufficient to fully represent the meteorological properties, especially in a rapidly evolving precipitation system. How to classify and group the precipitation features in a more dynamic way is still under development.

2) VPR Correction: Fig. 3(a) shows the VPR correction scheme for WSR-88D measurements using the S-PROF data as a reference. Spatially, the reflectivity observations from a single S-PROF are assumed to represent the vertical structure of reflectivity in each subdomain. Temporally, the S-PROF produces a vertical measurement every minute, whereas it takes 5–6 min for a WSR-88D to finish a volume scan. Therefore, the S-PROF observations are averaged across two adjacent KDAX radar scans (forward and backward in time: ∼10-minute window), and the averaged S-PROF data are directly used to represent the KDAX radar reflectivity pattern for an individual scan [see Fig. 3(c)]. In addition, a moving average filter (window size is 10) is applied to the averaged S-PROF profiles in order to reduce the measurement fluctuations and other random errors.

As mentioned, the sampling volume of WSR-88D radar becomes very large at far ranges due to the beam broadening effect. The lowest scan tilt that is free from blockage is 1.3°, which is used in this article. Over the Russian River watershed, the spacing between the top and bottom of the KDAX radar's 1.3° beam spans from 1.2 to 2.3 km at different portions of the watershed. By contrast, the range spacing of the S-PROF is about 60 m. Therefore, the range gate [Z_P in Fig. 3(a)] closest to the center of the KDAX radar beam is selected from the S-PROF observations to compare with the corresponding KDAX radar measurement. At the S-PROF location, the intersecting points between the KDAX radar's 1.3° beam center and the S-PROF sampling volumes are computed using the World Geodetic System 1984 Earth model. Then, the difference between the KDAX radar and the S-PROF reflectivity is calculated at the intersect points and used for the correction. Similarly, at other locations within the same

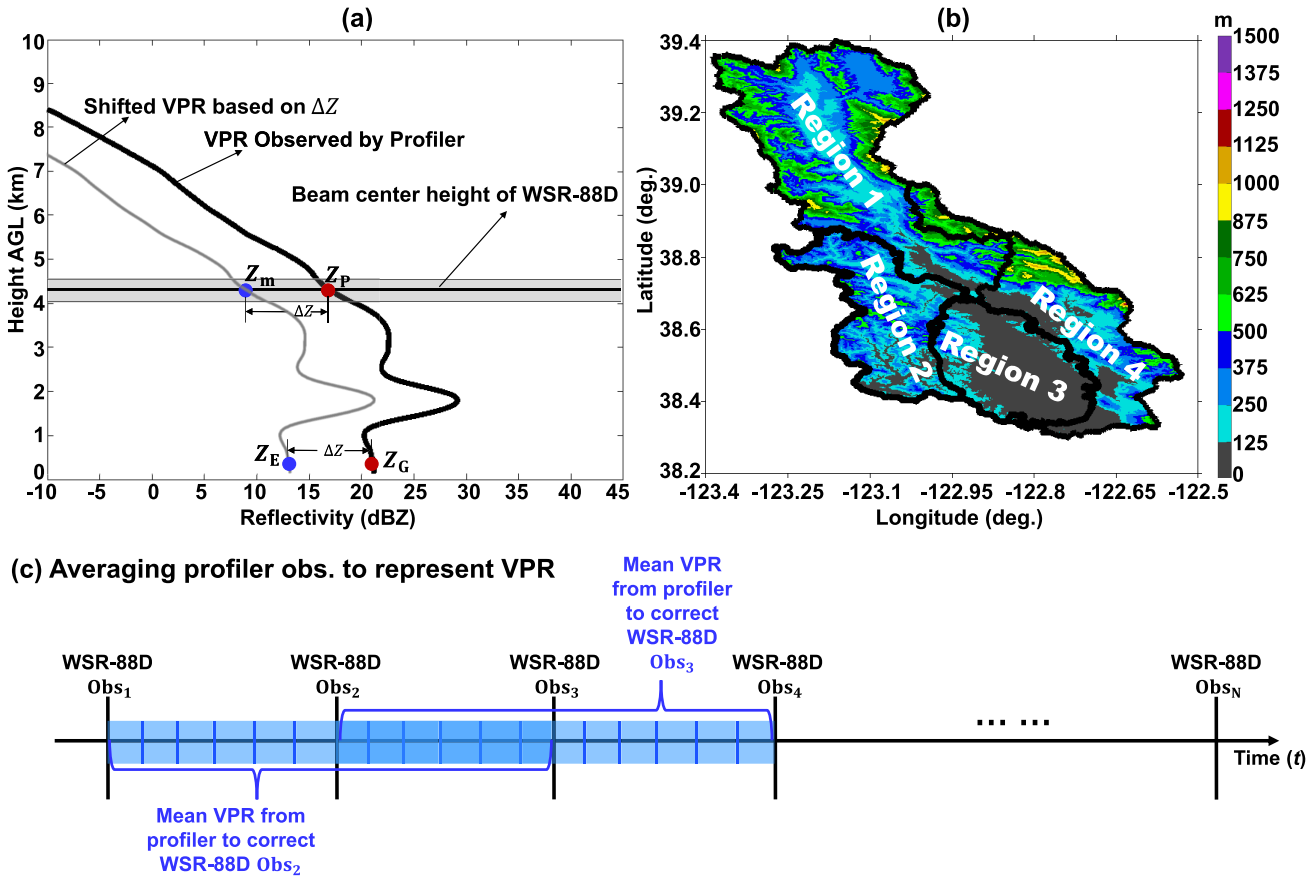

Fig. 3. (a) VPR correction scheme for scanning radar measurements based on the vertically pointing profiler radar observations. The black curve represents VPR observed by the profiler radar, whereas the gray curve with the same pattern denotes the shifted VPR to match scanning radar observations at the same height. (b) Example clustered regions derived from terrain information. The vertical structures of precipitation over these regions will be represented by VPR observations from the four profilers shown in Fig. 1(b). (c) Temporal averaging of high-resolution profiler data to generate representative VPR signatures for scanning radar measurements at a coarser resolution. $\text{Obs}_1 \cdots \text{Obs}_N$ stand for the WSR-88D observations.

subdomain, the same VPR curve observed by the profiler is used. The difference between the scanning WSR-88D radar (KDAX in this case) reflectivity measurement aloft and profiler data collected at the same height with the KDAX radar sampling volume at a given location is computed and used for subsequent correction.

It should be noted that only the VPR curve/shape is assumed to be the same within each subdomain identified through the clustering technique mentioned previously. At each grid cell in the subdomain, the VPR curve observed by the profiler is shifted according to the difference between the profiler and KDAX measurements at the same height until the VPR curve intersects with the reflectivity value observed by the KDAX radar. The ground-level reflectivity (i.e., Z_E) to be observed by the KDAX radar is determined by the actual measurement aloft and the differences

$$\Delta Z = Z_m - Z_p \tag{1a}$$

$$Z_E = Z_G + \Delta Z \tag{1b}$$

where Z_m is the scanning radar reflectivity measurement at a given location, Z_P is the reflectivity measurement at the same height but from the vertically pointing profiler radar, Z_G is the corresponding profiler radar reflectivity measurement near the surface, and Z_E is the VPR-corrected KDAX radar reflectivity close to the ground. In this article, the profiler radar measurement Z_G is selected at the third range gate from the ground (~300-m AGL) to avoid possible ground clutters at lower heights.

3) Radar Rainfall Relation: In order to demonstrate the performance of the proposed VPR correction scheme, instantaneous rain rates are derived from both the reflectivity before and after VPR correction for the preselected KDAX scan.

In particular, radar rainfall relations applied in the operational MRMS system [14] are adopted to derive the QPE products for this particular domain. The rainfall relations are as follows:

$$R = \max(0.0365Z^{0.625}, 0.1155Z^{0.5}) \tag{2a}$$

$$R = 0.017Z^{0.714} \tag{2b}$$

$$R = 0.1155Z^{0.5} \tag{2c}$$

where (2a) is for warm and cold stratiform rain, (2b) is for convective rain and hail, and (2c) is for snow; Z represents the radar reflectivity ($\text{mm}^6\ \text{m}^{-3}$), and R stands for rain rate [see (2a) and (2b)] or the melted equivalent snowfall rate [see (2c)] (mm h^{-1}).

The rain rates are then aggregated to derive hourly rainfall estimates. The rain gauge data at hourly scale are used to

verify the VPR correction performance and quantitatively evaluate various hourly rainfall products derived from the radar. It should be noted that the relations in (2) are adopted mainly because of the desire to compare with the QPE performance of operational products (i.e., MRMS) currently available in this region. In addition, (2a) is predominantly used for most of the rainfall events over this complex terrain. A detailed precipitation microphysics study is underway to find more suitable $Z-R$ relationships, which can better represent local precipitation characteristics, and they are expected to produce relatively improved QPE. Furthermore, since the WSR-88D systems are upgraded with dual-polarization capability, the application of polarimetric radar rainfall methodologies (see [27], [28]) should be considered in the future, especially in the regions below the BB.

III. Case Studies and Results

A. Precipitation Events

In this section, the QPE results are presented using two case studies to test the performance of the VPR correction methodology. After several years of drought conditions, California received abundant precipitation in the 2017 water year, setting the wettest year on record [19]. More than half of the precipitation fell in January and February, making the combined two-month rainfall total the highest in Januaries and Februaries ever recorded in Northern California. Within this period, there were several discrete multiday, heavy precipitation events that substantially helped to eliminate the drought situation. However, heavy precipitation also caused major floods, mudslides, and debris flows. In this article, the AR events were first identified using the satellite-derived integrated water vapor (IWV) data [29]. As expected, all precipitation occurred in January and February of 2017 was associated with AR phenomenon. The two major events that impacted the Russian River watershed and produced flooding in the region are analyzed in this article: January 8 and February 7 cases. In particular, the KDAX radar and S-PROF data collected during intense rainfall periods (i.e., January 8, 2017 00UTC–January 11, 2017 00UTC for the first event; February 7, 2017 00UTC–February 10, 2017 00UTC for the second event) are used to demonstrate the proposed VPR correction scheme. As typical AR events, the two case studies presented in this article can represent the local precipitation characteristics to a large extent [17], [19].

During the first event, Sonoma County was especially hit by the above-noted storms, and many vineyards along the Russian River watershed were flooded. Fig. 4(a) shows the vertical structure of reflectivity observed by the four profiler radars on January 10, 2017. On this particular day, the BB heights were about 1-, 1.5-, 1.1-, and 0.5-km AGL before 12UTC at Cazadero (CZC), Santa Rosa (STR), Hopland (HOP), and Middletown (MDT), respectively. The BB levels at all the four stations were slightly elevated after 12UTC, likely due to the diurnal change (BB level is higher during daytime because of the higher temperature). The second event coincided with the near failure of the Oroville Dam farther east in the Feather River Basin of the Sierra. It is worth noting that Oroville Dam's main and emergency spillways were damaged due to the large volume of water, prompting the evacuation of 188 000 people living downstream along the Feather River. A comprehensive study of the Oroville flood event can be found in [19]. In the Russian River watershed, the February event was associated with two consecutive ARs producing persistent heavy precipitation. Fig. 4(b) shows sample observations from the four profiler radars during this event. The BB heights are about 1.4-, 2-, 1.5-, and 0.8-km AGL at CZC, STR, HOP, and MDT, respectively. After 06UTC, the BB levels are eventually elevated to about 2, 2.9, 2, and 1 km at the four sites, respectively.

The differences in the reflectivity profile characteristics for both events shown in Fig. 4 over relatively short distances emphasize the complexity of rainfall processes resulting from orographic enhancement as well as the need for the ancillary profiler observations to improve the WSR-88D QPE. In Section III-B the VPR correction performance will be quantified in terms of QPE.

B. Results

Fig. 5 shows an example of the impact of the VPR correction on the KDAX radar reflectivity across the Russian River watershed. Overall, the KDAX radar reflectivity is greatly enhanced after VPR correction, particularly in the regions characterized by high mountains (see Fig. 2 for a watershed terrain map). In addition, since the watershed is very far from the KDAX radar, the elevated beam height and beam broadening effect severely degrade the KDAX data quality. This is shown in Fig. 5(a) by the large radar reflectivity gradient extending from the southeast to the northwest part of the basin. The spurious radar reflectivity pattern is caused by the KDAX beam passing through the BB region near the southeast boundary (high reflectivity) and near the cloud top (low reflectivity) at the far northwest end of the watershed. This, again, indicates the challenges of using higher tilt angles for QPE, especially during shallow rainfall events [24]. However, this effect is significantly improved after VPR correction, as shown by the more realistic observations in Fig. 5(b). Fig. 5(b) also shows that the gradient between different subbasins is fairly smooth after the VPR correction is applied, except that near the boundary between Region 1 and Region 4. This implies that the proposed VPR correction scheme can capture most of the spatial variabilities of precipitation in this complex terrain region. The relatively sharp boundary between Region 1 and Region 4 is mainly caused by the steep mountain slope in that area. This problem may be alleviated by a more sophisticated clustering method; however, that work is beyond the scope of this article.

To illustrate the impact of the VPR correction on QPE, Fig. 6 shows sample rainfall accumulations at two gauge stations during a 12-h period on January 10, 2017 and February 7, 2017: one location (STR: left) with collocated S-PROF observations and one location (HLD: right) some distance from the nearest profiler observation. In other words, the direct profiler measurements are used to correct KDAX radar measurements at the STR station, while the VPR

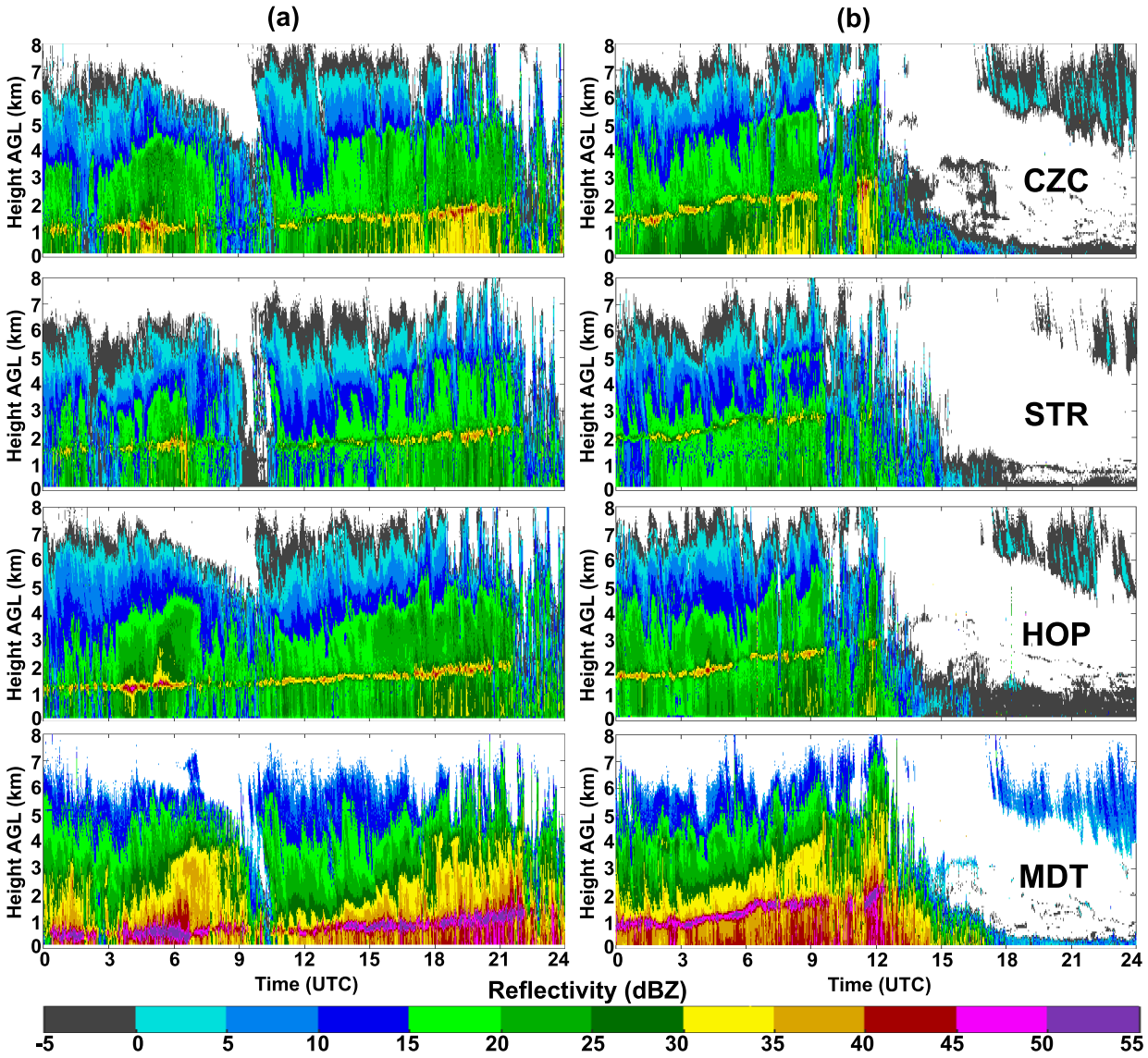

Fig. 4. Profiler reflectivity observations during the two precipitation events in 2017. (From Top to Bottom) Rows refer to the profiler site at CZC, STR, HOP, and MDT. (a) January 10, 2017. (b) February 7, 2017.

correction at the HLD site is based on the VPR structure generated from a nearby profiler (HOP in this case) that used to represent the whole Region 1 subbasin. Overall, dramatic improvement in rainfall estimation is observed after VPR correction at both sites. The corresponding MRMS radar-only products are also shown in Fig. 6 for comparison. Over this watershed, the MRMS radar-only products are predominantly derived from the same 1.3° elevation angle scans of the KDAX radar. However, different from using multiple VPR representatives, MRMS accounts for VPR in a conventional way [2], [13], [14]. That is, a single VPR curve was constructed in a mean sense in the MRMS system using the KDAX radar data, and this single VPR structure was applied in the whole domain covered by the KDAX radar for the correction of the reflectivity measurements.

In order to further quantify the improved rainfall performance after VPR correction, the data from all 35 gauges are used for both events, and the following metrics are computed at the common grid points between radar observations and gauge QPE measurements, including the normalized mean bias (NB), normalized standard error (NSE), Pearson's correlation coefficient (CORR), and the root-mean-square error (RMSE)

$$\mathrm{NB} = \frac{< R_E - R_G >}{< R_G >} \tag{3a}$$

$$\mathrm{NSE} = \frac{< |R_E - R_G| >}{< R_G >} \tag{3b}$$

$$\mathrm{CORR} = \frac{\sum[(R_E - < R_E >)(R_G - < R_G >)]}{\sqrt{\sum(R_E - < R_E >)^2}\sqrt{\sum(R_G - < R_G >)^2}} \tag{3c}$$

$$\mathrm{RMSE} = \sqrt{< (R_E - R_G)^2 >} \tag{3d}$$

where R_E is the QPE estimate from radar, R_G is the validation gauge measurement, and the angle brackets stand for the sample average.

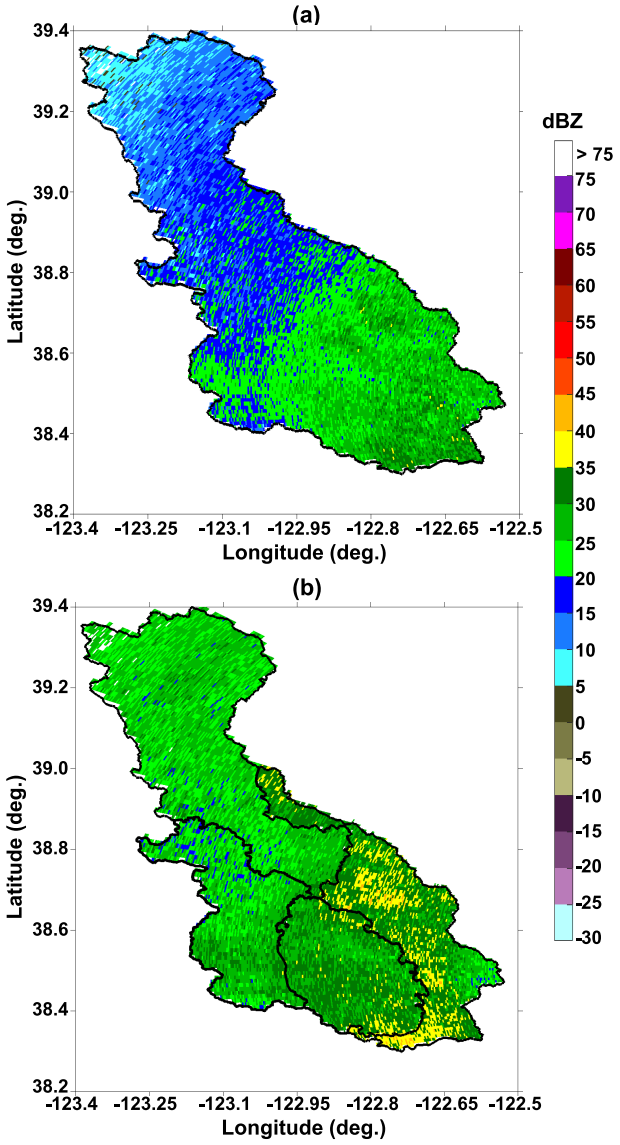

Fig. 5. KDAX radar reflectivity measurements at 1.3° scan elevation angle over the Russian River watershed on February 7, 2017 at 0459UTC (a) before and (b) after VPR correction.

TABLE IV

EVALUATION RESULTS OF HOURLY RAINFALL ESTIMATES FOR JANUARY 8, 2017 AND FEBRUARY 7, 2017 EVENTS

Hourly Rainfall Estimates	*NB*	*NSE*	*CORR*	*RMSE* (mm)
At all 35 gauge locations				
Radar w/o VPR Correction	-64.4%	65.3%	0.52	5.5
MRMS Radar-only	-64.8%	68.1%	0.43	5.7
Radar w/ VPR Correction	-32.1%	43.2%	0.59	3.9
At four gauge locations collocated with S-PROF				
Radar w/o VPR Correction	-46.2%	48.5%	0.76	3.2
MRMS Radar-only	-49.2%	57.3%	0.62	3.7
Radar w/ VPR Correction	-10.2%	41.4%	0.64	2.6

The overall evaluation results of hourly rainfall products during these two events are shown in Table IV and are further shown in Fig. 7. It should be noted that the evaluation scores are computed both for all the 35 gauge locations and for only the four gauge stations where the collocated profiler data are available. Table IV shows that the rainfall estimates before VPR correction involve substantial underestimation compared with the surface gauge measurements. This is in line with the findings in a previous study which used KDAX and KMUX for QPE in the Russian River watershed [24]. The performance of MRMS radar-only product derived based on the conventional VPR correction using a single vertical profile is very close to the estimates without accounting for VPR correction. The differences are not statistically significant, although the MRMS radar-only products show a little less underestimation (i.e., slightly better performance) at some gauge locations such as the one shown in Fig. 6(b). The QPE performance after applying the new VPR correction method is much better than that before VPR correction in terms of all the evaluation metrics. In addition, the results at the four gauge stations collocated with profiler radars exhibit better performance than the overall scores for all 35 stations. This is mainly because more direct measurements are available at those four gauge stations. Nevertheless, the overall performance is still promising, particularly given that most of the stations are not equipped with profiler radars.

C. Discussion

Based on the two case studies, it is concluded that the innovative VPR correction scheme described in this article performs much better than conventional VPR correction approach. The normalized standard error of hourly rainfall estimates is improved by about 20% (i.e., overall performance at all gauge locations) after applying this multiple S-PROF based correction methodology. However, it should be noted that the proposed method still has limitations during shallow non-BB (NBB) rain events. Since the WSR-88D radars are deployed quite far from this watershed, it is entirely possible that no precipitation echoes will be detected during shallow NBB rain due to beam overshooting, even it is raining at the ground. Unfortunately, such shallow NBB events do occur and account for 12%–15% of the total precipitation in this region as documented by Matrosov *et al.* [24]. The conventional VPR correction approaches, either based on a long-term climatological VPR curve or the short-term observed VPR curves, also have this limitation when applied in shallow NBB rain scenarios. One possible solution to this problem is to deploy high-resolution gap-filling radars to better sample the atmosphere closer to the surface [7].

In addition, extra attention should be paid to the broad application of the proposed approach in other domains. On the one hand, not every basin has multiple profilers as the NOAA HMT. In fact, there may be no radar information additional to WSR-88D. On the other hand, the local climatological properties can be very different from those in Northern California. In these cases, it is suggested that one can combine both the WSR-88D data and model output such as the high-resolution rapid refresh (HRRR) [30] to resolve the differences in the vertical structure of precipitation and subsequently derive the

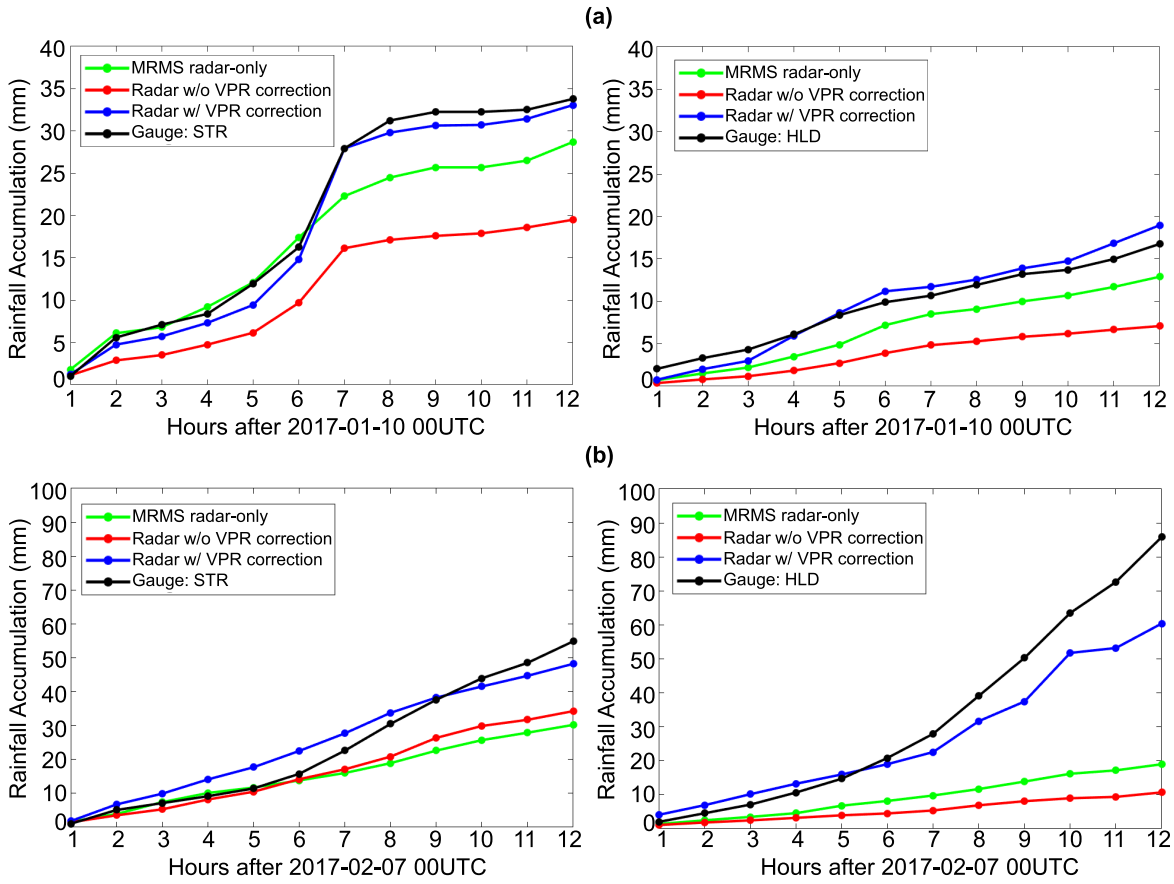

Fig. 6. Rainfall accumulations at two rain gauge stations during a 12-h period on (a) January 10, 2017 and (b) February 7, 2017. The station on the left (i.e., STR) is equipped with a profiler radar, which is used to correct KDAX radar measurements at this location. There is no collocated profiler data available at the station on the right (i.e., HLD), in which case the VPR correction is based on the representative VPR structure generated from a nearby profiler.

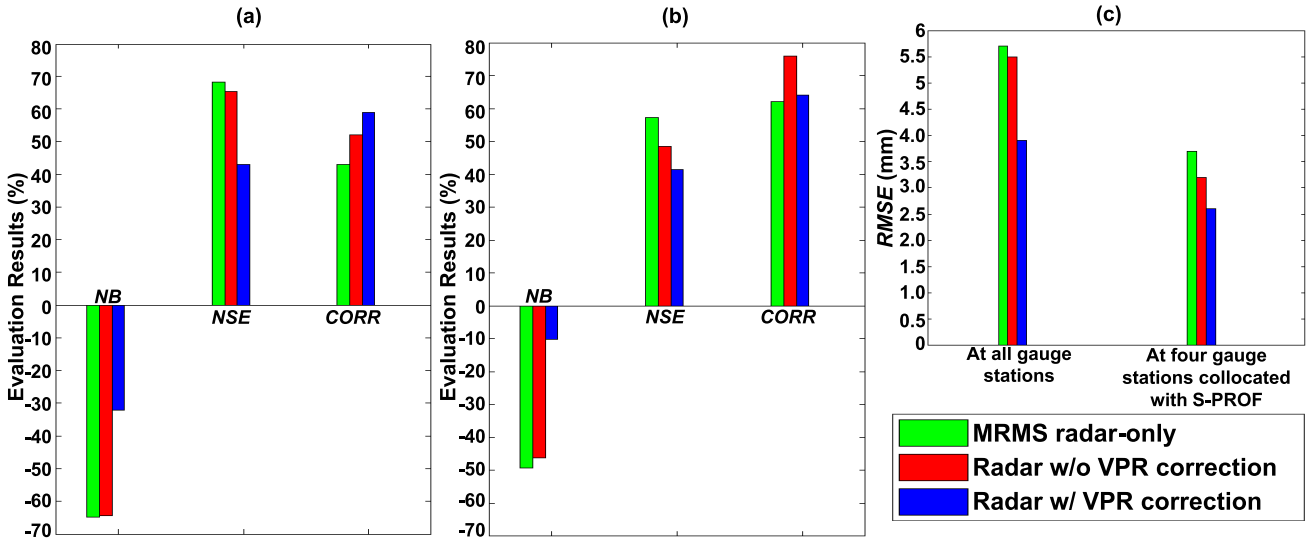

Fig. 7. Quantitative evaluation results of hourly rainfall estimates for January 8, 2017 and February 7, 2017 events combined. (a) Performance at all 35 gauge locations. Note that there is no profiler data available at 31 of the 35 gauge stations. (b) Performance at four gauge stations where the collocated profiler data are available. (c) RMSE (the lower the better) of hourly rainfall estimates. The scores in (a) and (b) include NB (the lower the better), NSE (the lower the better), and CORR (the higher the better).

VPR curves that can better represent the spatial characteristics than the conventional (mean) VPR.

IV. Conclusion

Despite recent advances in radar meteorology, the operational NWS radar network still has significant limitations for QPE over the western U.S. due to the fundamental coverage gaps [1], [3], [14], [31]. In addition to the large distances between the NWS radar sites, partial beam blockage caused by mountainous terrain at low elevation angles extends the challenges for QPE [24], [32]. Unfortunately, a number of flood-prone river basins, including those in Northern California,

are in the areas of poor radar coverage. Therefore, improving operational radar-based QPE is critical to stream hydrology and the protection of aquatic ecosystems. The improved QPE can also result in better flood forecasting [33].

This article introduced an innovative methodology for correcting the VPR observed by the operational radar in complex terrain. In particular, the reflectivity profiles measured by a number of high-resolution vertically pointing profiler radars were used as references of the vertical structure of precipitation. Spatially, a clustering analysis based on the terrain information was conducted to characterize the spatial representativeness of different profilers. Temporally, multiple high-resolution vertical samples of profiler radar were aggregated to guide the operational radar data processing. A demonstration study has been performed over the Russian River watershed in Northern California; therein, the VPR correction for operational scanning radar takes into account the temporal and spatial variations of precipitation at different subbasins. It was shown that the VPR adjustments using a combination of profilers produced better QPE than using a single VPR curve to correct observations over the entire basin.

Two typical AR events in January and February of 2017 were analyzed to demonstrate the proposed VPR correction scheme. The VPR correction performance has been quantified in terms of QPE. The results show that the QPE performance is significantly improved after VPR correction. With the aid of such auxiliary profiler observations, operational QPE products could be improved for this region. As part of our continuing effort to improve radar QPE over complex terrain, future work will focus on the bias correction of the improved QPE product using extensive gauge observations. In addition, the terrain-based clustering method used to determine which profiler station can represent a subbasin climatology was purely derived from the hydrologic perspective. Meteorological considerations, as well as the impacts of distance from the profilers, should be included in the future to further capture the spatial variability in precipitation, especially in the subdomains characterized by steep mountain slopes.

ACKNOWLEDGMENT

The authors are would like to thank Dr. S. Matrosov and three anonymous reviewers for their careful review and comments on this article. They would also like to thank NOAA/PSD engineers P. Johnston, S. Abbott, T. Ayers, C. King, and J. Leach for installing and maintaining the hydrometeorological instruments used in this article.

REFERENCES

[1] R. A. Maddox, J. Zhang, J. J. Gourley, and K. W. Howard, "Weather radar coverage over the contiguous United States," *Weather Forecasting*, vol. 17, pp. 927–934, Aug. 2002.

[2] J. Zhang, Y. Qi, D. Kingsmill, and K. Howard, "Radar-based quantitative precipitation estimation for the cool season in complex terrain: Case studies from the NOAA hydrometeorology testbed," *J. Hydrometeor.*, vol. 13, pp. 1836–1854, Dec. 2012.

[3] D. Willie *et al.*, "Evaluation of multisensory quantitative precipitation estimation in Russian river basin," *J. Hydrol. Eng.*, vol. 22, no. 5, p. E5016002, 2017.

[4] H. Chen, R. Cifelli, V. Chandrasekar, and Y. Ma, "A flexible Bayesian approach to bias correction of radar-derived precipitation estimates over complex terrain: Model design and initial verification," *J. Hydrometeorol.*, to be published.

[5] A. B. White, P. J. Neiman, F. M. Ralph, D. E. Kingsmill, and P. O. Persson, "Coastal orographic rainfall processes observed by radar during the California Land-Falling Jets Experiment," *J. Hydrometeor.*, vol. 4, pp. 264–282, 2003.

[6] R. A. Houze, Jr., "Orographic effects on precipitating clouds," *Rev. Geophysics*, vol. 50, no. 1, p. RG1001, 2012.

[7] R. Cifelli, V. Chandrasekar, H. Chen, and L. E. Johnson, "High resolution radar quantitative precipitation estimation in the San Francisco Bay Area: Rainfall monitoring for the urban environment," *J. Meteorolog. Soc. Jpn.*, vol. 96A, pp. 141–155, May 2018.

[8] S. Y. Matrosov, K. A. Clark, and D. E. Kingsmill, "A polarimetric radar approach to identify rain, melting-layer, and snow regions for applying corrections to vertical profiles of reflectivity," *J. Appl. Meteor. Climatol.*, vol. 46, no. 2, pp. 154–166, 2007.

[9] M. Kitchen, R. Brown, and A. G. Davies, "Real-time correction of weather radar data for the effects of bright band, range and orographic growth in widespread precipitation," *Quart. J. Royal Meteorol. Soc.*, vol. 120, no. 519, pp. 1231–1254, 1994.

[10] H. C. Andrieu and J. Dominique, "Identification of vertical profiles of radar reflectivity for hydrological applications using an inverse method. Part I: Formulation," *J. Appl. Meteorol.*, vol. 34, no. 1, pp. 225–239, 1995.

[11] U. Germann and J. Joss, "Mesobeta profiles to extrapolate radar precipitation measurements above the Alps to the ground level," *J. Appl. Meteorol.*, vol. 41, no. 5, pp. 542–557, May 2002.

[12] A. Bellon, G. W. Lee, and I. Zawadzki, "Error statistics of VPR corrections in stratiform precipitation," *J. Appl. Meteor.*, vol. 44, pp. 998–1015, Jul. 2005.

[13] J. Zhang and Y. Qi, "A real-time algorithm for the correction of brightband effects in radar-derived QPE," *J. Hydrometeor.*, vol. 11, pp. 1157–1171, Oct. 2010.

[14] J. Zhang *et al.*, "National Mosaic and multi-sensor QPE (NMQ) system: Description, results, and future plans," *Bull. Amer. Meteorolog. Soc.*, vol. 92, pp. 1321–1338, Oct. 2011.

[15] J. Koistinen and H. Pohjola, "Estimation of ground-level reflectivity factor in operational weather radar networks using vpr-based correction ensembles," *J. Appl. Meteor. Climatol.*, vol. 53, pp. 2394–2411, Oct. 2014.

[16] Y. Qi, J. Zhang, B. Kaney, C. Langston, and K. Howard, "Improving WSR-88D radar QPE for orographic precipitation using profiler observations," *J. Hydrometeor.*, vol. 15, pp. 1135–1151, Jun. 2014.

[17] F. M. Ralph *et al.*, "Flooding on California's Russian river: Role of atmospheric rivers," *Geophys. Res. Lett.*, vol. 33, no. 13, p. L13801, 2006.

[18] R. E. Newell, N. E. Newell, Y. Zhu, and C. Scott, "Tropospheric rivers?—A pilot study," *Geophys. Res. Lett.*, vol. 19, no. 24, pp. 2401–2404, 1992.

[19] A. B. White, B. J. Moore, D. J. Gottas, and P. J. Neiman, "Winter storm conditions leading to excessive runoff above California's Oroville dam during January and February 2017," *Bull. Amer. Meteor. Soc.*, vol. 100, pp. 55–70, Feb. 2019.

[20] A. B. White *et al.*, "A twenty–first century California observing network for monitoring extreme weather events," *J. Atmos. Ocean. Technol.*, vol. 30, no. 8, pp. 1585–1603, 2013.

[21] A. B. White, J. R. Jordan, B. E. Martner, F. M. Ralph, and B. W. Bartram, "Extending the dynamic range of an S-band radar for cloud and precipitation studies," *J. Atmos. Ocean. Technol.*, vol. 17, pp. 1226–1234, Sep. 2000.

[22] D. E. Kingsmill, P. J. Neiman, F. M. Ralph, and A. B. White, "Synoptic and topographic variability of northern California precipitation characteristics in landfalling winter storms observed during CALJET," *Monthly Weather Rev.*, vol. 134, no. 8, pp. 2072–2094, 2006.

[23] B. E. Martner, P. J. Neiman, and A. B. White, "Collocated radar and radiosonde observations of a double-brightband melting layer in northern California," *Monthly Weather Rev.*, vol. 135, pp. 2016–2024, May 2007.

[24] S. Y. Matrosov, F. M. Ralph, P. J. Neiman, and A. B. White, "Quantitative assessment of operational weather radar rainfall estimates over California's northern Sonoma county using HMT-west data," *J. Hydrometeor.*, vol. 15, pp. 393–410, Feb. 2014.

[25] S. K. Jenson and J. O. Domingue, "Extracting topographic structure from digital elevation data for geographic information system analysis," *Photogramm. Eng. Remote Sens.*, vol. 54, no. 11, pp. 1593–1600, 1988.

[26] R. C. Gonzalez and R. E. Woods, *Digital Image Processing*. Englewood Cliffs, NJ, USA: Prentice-Hall, 2002.
[27] R. Cifelli, V. Chandrasekar, S. Lim, P. C. Kennedy, Y. Wang, and S. A. Rutledge, "A new dual-polarization radar rainfall algorithm: Application in Colorado precipitation events," *J. Atmos. Ocean. Technol.*, vol. 28, pp. 352–364, Mar. 2011.
[28] H. Chen, V. Chandrasekar, and R. Bechini, "An improved dual-polarization radar rainfall algorithm (DROPS2.0): Application in NASA IFloodS field campaign," *J. Hydrometeorol.*, vol. 18, no. 4, pp. 917–937, 2017.
[29] F. M. Ralph, P. J. Neiman, and G. A. Wick, "Satellite and CALJET aircraft observations of atmospheric rivers over the eastern north pacific ocean during the winter of 1997/98," *Monthly Weather Rev.*, vol. 132, pp. 1721–1745, Jul. 2004.
[30] S. G. Benjamin *et al.*, "A North American hourly assimilation and model forecast cycle: The Rapid Refresh," *Monthly Weather Rev.*, vol. 144, pp. 1669–1694, Apr. 2016.
[31] J. Bytheway, M. Hughes, K. Mahoney, and R. Cifelli, "A multiscale evaluation of multisensor quantitative precipitation estimates in the Russian river basin," *J. Hydrometeor.*, vol. 20, pp. 447–466, Mar. 2019.
[32] Y. B. Gou, Y. Ma, H. Chen, and Y. Wen, "Radar-derived quantitative precipitation estimation in complex terrain over the eastern tibetan plateau," *Atmos. Res.*, vol. 203, pp. 286–297, May 2018.
[33] M. D. Dettinger, F. M. Ralph, T. Das, P. J. Neiman, and D. R. Cayan, "Atmospheric rivers, floods and the water resources of California," *Water*, vol. 3, no. 2, pp. 445–478, 2011.

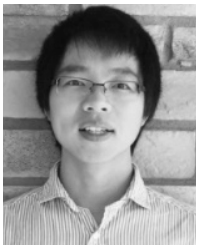

Haonan Chen (S'08–M'17) received the bachelor's degree from the Chongqing University of Posts and Telecommunications, Chongqing, China, in 2010, and the M.S. and Ph.D. degrees from Colorado State University (CSU), Fort Collins, CO, USA, in 2013 and 2017, respectively, all in electrical engineering.

He has been with the Physical Sciences Division, NOAA Earth System Research Laboratory, Boulder, CO, USA, since 2012, first as a Research Student, then a National Research Council Research Associate, and currently a Radar, Satellite, and Precipitation Scientist at the Co-operative Institute for Research in the Atmosphere (CIRA). He is also an Affiliate Faculty Member with the Department of Electrical and Computer Engineering, CSU. His research interests include advancing the understanding of the physical sciences in the hydrometeorological processes through remote sensing technologies. He specializes in radar systems and networking, precipitation classification and estimation with polarimetric radar measurements, and multiscale radar and satellite data fusion.

Dr. Chen serves as an Associate Editor for the *Journal of Atmospheric and Oceanic Technology*, an Associate Editor for *URSI Radio Science Bulletin*, and a Guest Editor for *Remote Sensing*.

Robert Cifelli received the bachelor's degree in geology from the University of Colorado Boulder, Boulder, CO, USA, in 1983, the M.S. degree in hydrogeology from West Virginia University, Morgantown, WV, USA, in 1986, and the Ph.D. degree in atmospheric science from Colorado State University, Fort Collins, CO, USA, in 1996.

He is a Radar Meteorologist with over 25 years of experience in precipitation research and over 60 publications in peer-reviewed journal articles. Since 2009, he has been leading NOAA scientists dedicated to improving precipitation and hydrologic prediction in complex terrain and other geographic regions. He currently leads the Hydrometeorology Modeling and Applications (HMA) Team, Physical Sciences Division, NOAA Earth System Research Laboratory, Boulder. A major focus of HMA is to improve understanding of physical processes represented in the National Water Model and to guide future model development. He completed a detail with the Bureau of Reclamation in 2016 through the President's Management Council Interagency Rotation Program. He continues to work closely with the Reclamation Research and Development Office on developing improved weather, climate, and water forecasts of extreme events to better meet water management needs. He also works closely with the NOAA Office of Water Prediction (OWP) on the evaluation of forcings for hydrologic prediction, physical process representation in the National Water Model, and coordination of quantitative precipitation estimation and forecast efforts across NOAA to address internal OWP and external stakeholder needs.

Allen White received the bachelor's degree in mechanical engineering from Brown University, Providence, RI, USA, in 1984, and the M.S. and Ph.D. degrees in meteorology from Pennsylvania State University, State College, PA, USA, in 1989 and 1996, respectively.

He is a Research Meteorologist with the NOAA Earth System Research Laboratory, Boulder, CO, USA, where he currently leads the Hydrometeorological Observations and Processes Team, Physical Sciences Division. He is also leading an effort to provide 21st-century observations, forecast models, display systems, and decision support tools to bear on California's water resource and flood management concerns. He has authored more than 80 scientific journal articles. He holds a U.S. patent for his research. His research interests include boundary layers and turbulence, coastal weather, precipitation science, air pollution meteorology, and instrument algorithm development.

Dr. White has received several awards.